RAA 2019 Vol. **19** No. **10**, 147(12pp) doi: 10.1088/1674–4527/19/10/147

http://www.raa-journal.org *http://iopscience.iop.org/raa*

Research in Astronomy and Astrophysics

Photometric investigations on two totally eclipsing contact binaries: V342 UMa and V509 Cam

Kai Li[1,2], Qi-Qi Xia[1], Jin-Zhong Liu[3], Yu Zhang[3], Xing Gao[3], Shao-Ming Hu[1], Di-Fu Guo[1], Xu Chen[1] and Yuan Liu[4]

[1] Shandong Provincial Key Laboratory of Optical Astronomy and Solar-Terrestrial Environment, Institute of Space Sciences, Shandong University, Weihai 264209, China; *kaili@sdu.edu.cn*
[2] Key Laboratory for the Structure and Evolution of Celestial Objects, Chinese Academy of Sciences, Kunming 650216, China
[3] Xinjiang Astronomical Observatory, Chinese Academy of Sciences, Urumqi 830011, China
[4] Qilu Institute of Technology, Jinan 250200, China

Received 2019 March 28; accepted 2019 May 28

Abstract By analyzing two sets of complete BVR_cI_c light curves for V342 UMa and three sets of complete BVR_cI_c light curves for V509 Cam, we determined that the two systems are both W-subtype contact binaries and that V342 UMa manifests a shallow contact configuration, while V509 Cam exhibits a medium contact configuration. Given that both of them are totally eclipsing binaries, the physical parameters derived only by the photometric light curves are reliable. Meanwhile, the period changes of the two targets were analyzed based on all available eclipsing times. We discovered that V342 UMa shows long-term period decrease with a rate of $-1.02(\pm0.54) \times 10^{-7}$ d yr^{-1} and that V509 Cam displays long-term period increase with a rate of $3.96(\pm0.90) \times 10^{-8}$ d yr^{-1}. Both the conservative mass transfer and angular momentum loss via magnetic stellar winds can be used to interpret the long-term period decrease of V342 UMa. The long-term period increase of V509 Cam can be explained by mass transfer from the less massive star to the more massive one. The absolute parameters of the two binaries were estimated according to their *Gaia* distances and our derived photometric solution results. This method can be extended to other contact binaries without radial velocities but with reliable photometric solutions. Their evolutionary states were investigated and we found that they reveal properties that are identical to other W-subtype contact systems.

Key words: stars: binaries: close — stars: binaries: eclipsing — stars: individual (V342 UMa, V509 Cam)

1 INTRODUCTION

W UMa contact binaries are comprised of two late-type stars with spectral types from F to K. The two component stars are sharing a common convective envelope and have nearly equal effective temperatures although their masses are very different. The analysis of W UMa contact binaries is very necessary for modern astrophysics because they are probes for understanding tidal interactions, energy exchange, mass transfer and angular momentum loss (AML). The formation, evolution, ultimate fate and magnetic activities of W UMa contact binaries are still debatable issues (e.g., Guinan & Bradstreet 1998; Bradstreet & Guinan 1994; Eggleton & Kisseleva-Eggleton 2006; Fabrycky & Tremaine 2007; Qian et al. 2006, 2007a, 2014, 2017, 2018). To resolve these issues, the determination of physical parameters for a large number of such type binaries is required.

The physical parameters, such as mass ratio, for partially eclipsing contact binaries are poorly estimated (e.g., Pribulla et al. 2003; Terrell & Wilson 2005). In addition, the spectroscopic mass ratio sometimes cannot be reliably derived according to their broadened and blended spectral lines (e.g., Dall & Schmidtobreick 2005; Rucinski 2010). By the study of contact binaries, for which both spectroscopic and photometric mass ratios have been calculated, Pribulla et al. (2003) discovered that the photometric mass ratios of totally eclipsing systems correspond to their spectroscopic ones. Terrell & Wilson (2005) determined a similar result by discussing the relationships between photometric and spectroscopic mass ratios. These results suggest that we can derive very precise and reliable physical

parameters for totally eclipsing contact binaries only by the photometric light curves. Thanks to the *Gaia* mission (Gaia Collaboration et al. 2018), the parallaxes of more than one billion stars have been obtained, which allows researchers to estimate the absolute parameters of contact binaries even if there are no radial velocity observations (e.g., Kjurkchieva et al. 2019a,b). Therefore, we chose two totally eclipsing binaries, V342 UMa and V509 Cam, to analyze their light curves and period variations, and estimate their absolute parameters.

V342 UMa was first discovered as a W UMa type binary by Nelson et al. (2004) during the observations of a nearby star BH UMa. The period of 0.343854 d, the color index of $B-V=0.64$ and spectral type of G3 were acquired. Their photometric study revealed that V342 UMa is a low mass ratio ($q=0.331$) W-subtype contact binary (the hotter component is the less massive one). It has been 15 years since the discovery and first photometric investigation of V342 UMa, therefore we decided to re-examine the light curves and orbital period changes of this target.

V509 Cam was first identified as an EW type eclipsing binary by Khruslov (2006) during a search for eclipsing binaries in Camelopardalis. He determined the variability amplitude of 0.6 mag and the orbital period of 0.35034 d. However, at present, neither the light curve synthesis nor period variation analysis has been carried out for this star. Therefore, we will analyze the light curves and orbital period variations of this target in this paper.

2 CCD OBSERVATIONS OF V342 UMA AND V509 CAM

Charge-coupled device (CCD) photometry of V342 UMa and V509 Cam was carried out from 2018 to 2019 using the Weihai Observatory 1.0-m telescope of Shandong University (WHOT, Hu et al. 2014), the Nanshan One-meter Widefield Telescope (NOWT, Liu et al. 2014) at the Nanshan Station of Xinjiang Astronomical Observatory, the 60-cm Ningbo Bureau of Education and Xinjiang Observatory Telescope (NEXT), and the 85-cm telescope at Xinglong Station of National Astronomical Observatories, Chinese Academy of Sciences (NAOC85-cm). Information about the observations is listed in Table 1. In order to record the observed images, $2\mathrm{k}\times 2\mathrm{k}$ CCD cameras were utilized for WHOT, NEXT and NAOC85-cm and a $4\mathrm{k}\times 4\mathrm{k}$ CCD camera was employed with NOWT. The fields of view were $12^{'}\times 12^{'}$ for WHOT, $1.3^{\circ}\times 1.3^{\circ}$ for NOWT, $22^{'}\times 22^{'}$ for NEXT and $32^{'}\times 32^{'}$ for NAOC85-cm. The effective subframe of NOWT was $30^{'}\times 30^{'}$ during the observations. The filters we used are standard Johnson-Cousins-Bessel BVR_cI_c systems. The standard IRAF routine was applied to process the observed data including zero and flat calibrations, and aperture photometry, then differential magnitudes between the target and comparison star and those between the comparison and check stars were obtained. The complete light curves of V342 UMa observed by NEXT and WHOT and those of V509 Cam acquired by NOWT and NEXT are illustrated in Figure 1 and Figure 2, respectively. As seen in these two figures, the two targets manifest EW type light curves, and very clear flat primary minima can be located. Based on our observations, six eclipsing minima were derived for V342 UMa, while 10 were obtained for V509 Cam. All the minima were calculated by the Kwee-van Woerden (K-W) method (Kwee & van Woerden 1956) and are listed in Table 2.

3 ORBITAL PERIOD VARIATIONS

Although both V342 UMa and V509 Cam have been identified as variables for more than 10 years, no one has yet analyzed their orbital period variations. Thus, we collected all published eclipsing times for V342 UMa and V509 Cam from literature, and listed them in Table 2. Moreover, the Wide Angle Search for Planets (WASP, Butters et al. 2010) project has observed V342 UMa, and we calculated two minima using the archive data, which are also listed in Table 2. Combining our newly observed ones, we obtained a total of 43 photoelectric or CCD eclipsing times for V342 UMa, and a total of 17 photoelectric or CCD eclipsing times for V509 Cam. Using the least-squares method, the linear ephemeris of V342 UMa taken from Nelson et al. (2004) was corrected to be

$$\begin{aligned}\mathrm{Min.I} =& 2453054.83723(\pm 0.00090)\\ &+ 0.34385184^{\mathrm{d}}(\pm 0.00000010)\mathrm{E},\end{aligned} \tag{1}$$

and the linear ephemeris of V509 Cam referenced from the $O-C$ Gateway[1] was amended to be

$$\begin{aligned}\mathrm{Min.I} =& 2451492.27572(\pm 0.00071)\\ &+ 0.35034717^{\mathrm{d}}(\pm 0.00000004)\mathrm{E}.\end{aligned} \tag{2}$$

All the $O-C$ values calculated by the two equations are listed in Table 2, and the corresponding curves are displayed in Figure 3. We can find that both V342 UMa and V509 Cam manifest a parabolic trend. Then, quadratic ephemerides were applied to fit the $O-C$ curves of the two targets,

$$\begin{aligned}\mathrm{Min.I} =& -0.00043(\pm 0.00095)\\ &+ 0.00000069(\pm 0.00000038)\mathrm{E}\\ &- 4.81(\pm 2.56)\times 10^{-11}\mathrm{E}^2,\end{aligned} \tag{3}$$

$$\begin{aligned}\mathrm{Min.I} =& -0.00127(\pm 0.00056)\\ &- 0.00000041(\pm 0.00000010)\mathrm{E}\\ &+ 1.90(\pm 0.43)\times 10^{-11}\mathrm{E}^2.\end{aligned} \tag{4}$$

[1] The website of $O-C$ Gateway is *http://var.astro.cz/ocgate/*.

Table 1 The Observational Log for V342 UMa and V509 Cam

Star	Date	Filter and Typical Exposure Time	Type	Uncertainty (mag)*	Telescope
V342 UMa	2018 Mar 29	R_c40s	minimum light	R_c0.011	WHOT
	2018 May 08	B80 s V60 s R_c40 s I_c40 s	light curve	B0.007 V0.006 R_c0.007 I_c0.009	NEXT
	2018 May 21	B80 s V60 s R_c40 s I_c40 s	light curve	B0.010 V0.007 R_c0.007 I_c0.010	NEXT
	2018 May 27	B80 s V60 s R_c40 s I_c40 s	light curve	B0.008 V0.006 R_c0.007 I_c0.008	NEXT
	2018 Dec 28	R_c30 s	minimum light	R_c0.005	NAOC85-cm
	2019 Jan 20	B120 s V60 s R_c35 s I_c25 s	light curve	B0.005 V0.005 R_c0.005 I_c0.005	WHOT
V509 Cam	2018 Feb 08	B36 s V22 s R_c13 s I_c12 s	light curve	B0.006 V0.006 R_c0.006 I_c0.005	NOWT
	2018 Mar 05	B25 s V25 s R_c25 s I_c25 s	minimum light	B0.010 V0.009 R_c0.008 I_c0.008	NOWT
	2018 Mar 06	B14 s V10 s R_c10 s I_c10 s	light curve	B0.006 V0.005 R_c0.005 I_c0.005	NOWT
	2018 Apr 15	B70 s V50 s R_c40 s I_c30 s	light curve	B0.007 V0.006 R_c0.005 I_c0.007	NEXT
	2018 Apr 23	B70 s V50 s R_c40 s I_c30 s	light curve	B0.006 V0.005 R_c0.005 I_c0.007	NEXT
	2019 Jan 21	R_c40 s	minimum light	R_c0.003	WHOT

* Uncertainties are the standard deviation of the differences between the comparison and check stars.

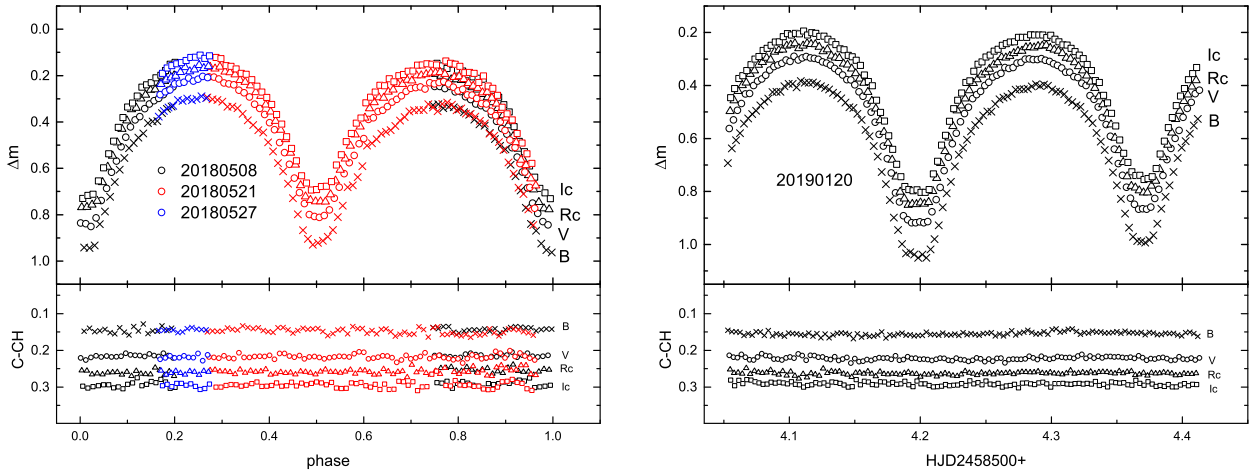

Fig. 1 The *left* panel displays the light curves of V342 UMa observed by NEXT on 2018 May 08, 21 and 27 (*black*, *red* and *blue symbols* respectively represent 20180508 observations, 20180521 observations and 20180527 observations), while the *right* panel depicts the light curves of V342 UMa observed by WHOT on 2019 Jan 20. *Crosses* refer to the B band light curves, while *open circles*, *triangles* and *squares* respectively represent the V, R_c and I_c band light curves.

When removing Equations (3) and (4), the residuals are listed in Table 2 and depicted in the bottom panels of Figure 3. No cyclic variations can be detected in the residuals. According to the coefficients of the quadratic terms in Equations (3) and (4), we determined that the period of V342 UMa is undergoing a secular decrease at a rate of $-1.02(\pm0.54)\times10^{-7}\,\mathrm{d\,yr^{-1}}$ and the period of V509 Cam is continuously increasing at a rate of $3.96(\pm0.90)\times10^{-8}\,\mathrm{d\,yr^{-1}}$.

4 PHOTOMETRIC SOLUTIONS OF V342 UMA AND V509 CAM

Based on our observations, two sets of complete light curves for V342 UMa and three sets of light curves for V509 Cam were obtained. The Wilson-Devinney (W-D) program (Wilson & Devinney 1971; Wilson 1979, 1990) was used to model these light curves. *Gaia* Data Release 2 (DR2, Gaia Collaboration et al. 2016, 2018) included these two targets with their determined mean temperatures, $T_m = 5741$ K for V342 UMa and $T_m = 6462$ K for V509 Cam. At first, the mean temperature was set as the temperature of the primary, T_1. The bolometric and bandpass limb-darkening coefficients were taken from van Hamme (1993)'s table, and the gravity-darkening coefficients and bolometric albedos were set as $g_{1,2} = 0.32$ and $A_{1,2} = 0.5$ respectively for their convective envelopes (Lucy 1967; Ruciński 1969). Due to the lack of radial velocity curves, the q-search method was applied to determine the mass ratios of the two systems. When we obtained the final solutions, the temperatures of the two components were calculated using the following method (Coughlin et al. 2011; Dimitrov & Kjurkchieva 2015),

$$\begin{aligned} T_1 &= T_m + \frac{c\Delta T}{c+1}, \\ T_2 &= T_1 - \Delta T, \end{aligned} \tag{5}$$

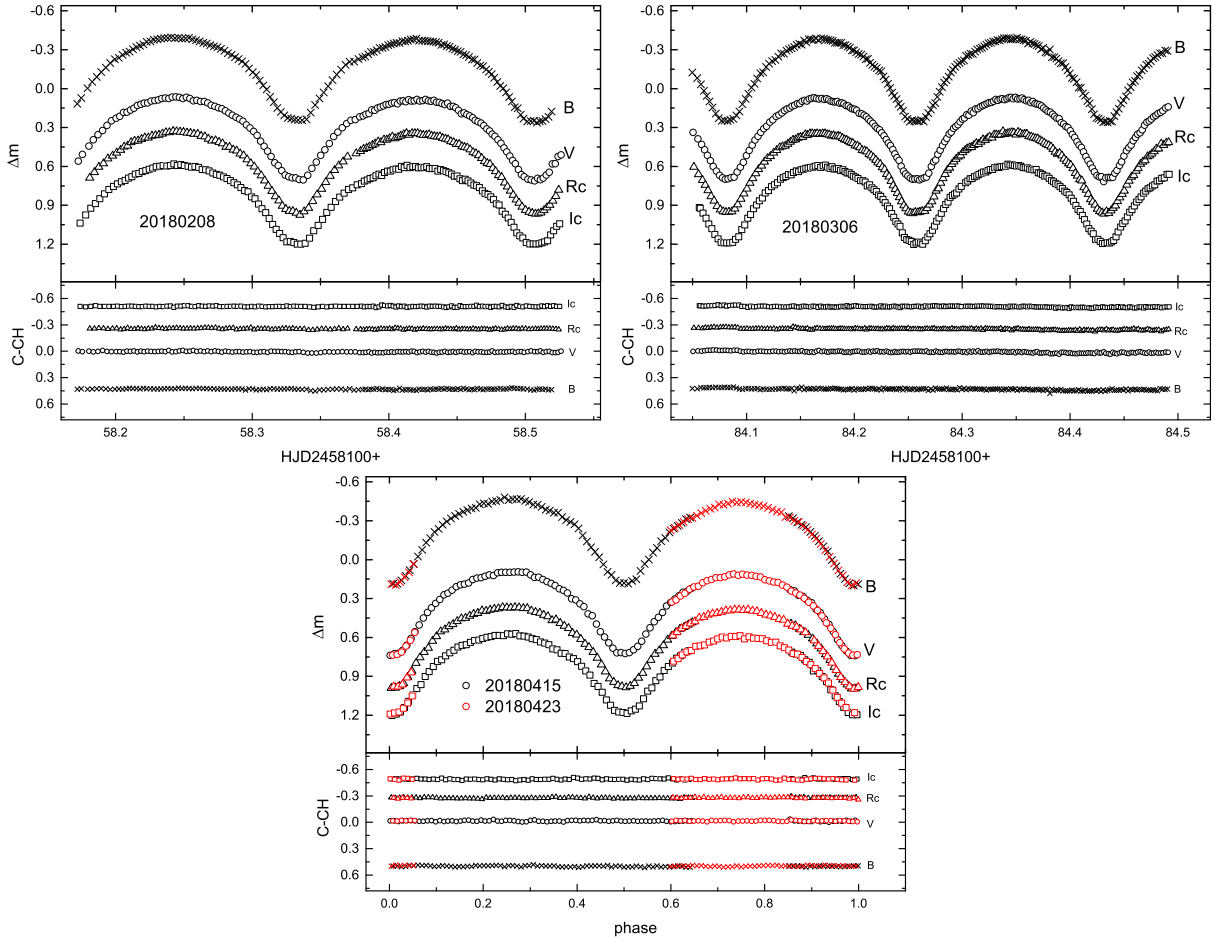

Fig. 2 The *upper left* panel displays the light curves of V509 Cam observed by NOWT on 2018 February 08, the *upper right* panel shows the light curves of V509 Cam acquired by NOWT on 2018 Mar 06, while the *bottom* panel plots the light curves of V509 Cam collected by NEXT on 2018 April 15 and 23 (*black* and *red symbols* respectively represent 20180415 observations and 20180423 observations). *Crosses* refer to the B band light curves, while *open circles*, *triangles* and *squares* respectively represent the V, R_c and I_c band light curves.

where $\Delta T = T_1 - T_2$ and $c = L_2/L_1$ are derived by the W-D modeling.

Because two or more sets of complete light curves were acquired for both V342 UMa and V509 Cam, and the light curves observed at different times are different, the physical parameters determined by different light curves may be different. Therefore, we chose one set of complete light curves to determine the physical parameters, and the derived physical parameters were set as reference values to model the other light curves. For V342 UMa, the complete light curves observed in 2019 have higher quality comparing to those observed in 2018, so the 2019 light curve was selected. For V509 Cam, the complete light curves observed on 2018 March 06 are symmetric and have the highest precision among the three sets of light curves, so the 201803 light curve was selected. During the modeling, we used Mode 2 (detached configuration) for both targets at first and found that the solutions were quickly convergent at Mode 3 (contact configuration). The adjustable parameters were as follows: the orbital inclination, i, the temperature of the secondary, T_2, the dimensionless potential of the primary Ω_1 and the monochromatic luminosity of the primary, L_1. Then, a series of solutions with fixed values of mass ratio q was generated for them. The weighted sum of squared residuals, $\sum W_i(O-C)_i^2$, versus mass ratio q for V342 UMa and V509 Cam are, respectively, displayed in the left and right panels of Figure 4. As seen in Figure 4, a very sharp minimum was determined for V342 UMa at $q = 2.8$, while that derived for V509 Cam was at $q = 2.5$. These two values were set as initial values, and adjustable parameters and new solutions were calculated. When the solutions were convergent, the physical parameters were obtained. The light curves of V342 UMa were asymmetric, and adding a cool spot on the less massive primary component could reproduce the asymmetric light curves. The derived physical parameters are listed in Table 3, and the corresponding synthetic light curves are plotted in Figure 5 and Figure 6.

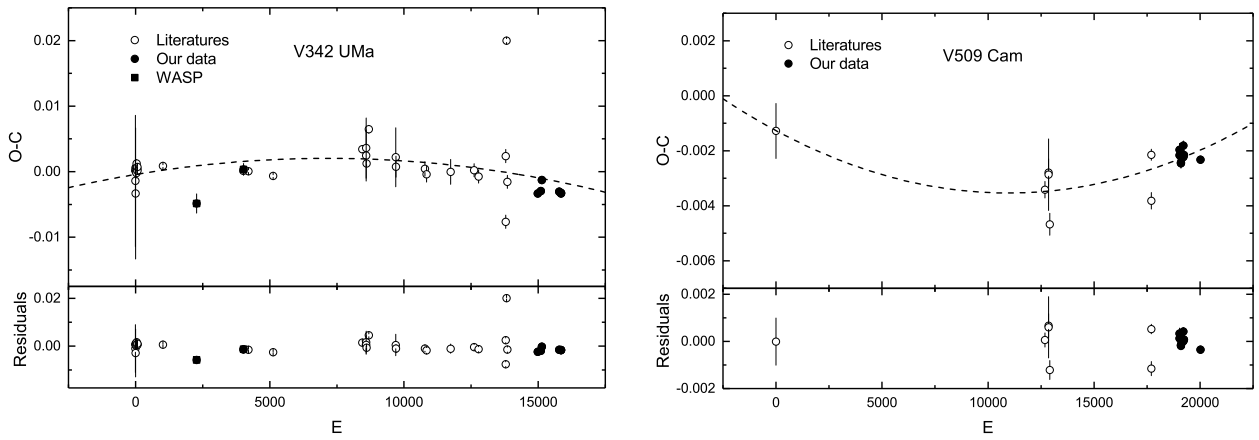

Fig. 3 The *left* panel displays the $O-C$ curve of V342 UMa, while the *right* panel depicts the $O-C$ curve of V509 Cam. *Open circles* refer to eclipsing times from the literature, *solid circles* represent our data, while *solid squares* signify the WASP eclipsing times. The errors of some points were not given in the literature and are fixed at 0.0010 when plotting this figure.

To model the other light curves, the physical parameters derived earlier were set as reference values and the mass ratio q was fixed. Because the light curves are asymmetric, a spot model was applied. The best fitting results are also displayed in Table 3, and the corresponding fitting curves are respectively displayed in Figure 5 and Figure 6. According to the previous discussion, the physical parameters determined by the 2019 light curve of V342 UMa and the 201803 light curve of V509 Cam should be more reliable. Therefore, the physical parameters determined by the 2019 light curve of V342 UMa and the 201803 light curve of V509 Cam were adopted as the final results. The geometric configurations of the two systems are, respectively, plotted in Figure 7 and Figure 8, and changes in the spot distributions can be clearly ascertained.

5 DISCUSSION AND CONCLUSIONS

Two sets of complete BVR_cI_c light curves for V789 Her and three sets of complete BVR_cI_c light curves for V509 Cam were obtained and analyzed. We discovered that both of these two systems are W-subtype contact binaries, with $q = 2.748 \pm 0.015$ for V342 UMa and $q = 2.549 \pm 0.016$ for V509 Cam. V342 UMa is a shallow contact binary with a fill-out factor of $f = 10.0 \pm 3.1\%$, and V509 Cam is a medium contact binary with a contact degree of $f = 32.1 \pm 3.4\%$. The two systems show totally eclipsing primary minima, their inclinations are higher than 82° and the q-search curves exhibit very clear sharpness around the bottom. This indicates that the photometric solutions derived only by the photometric light curves are reliable (e.g., Pribulla et al. 2003; Terrell & Wilson 2005; Zhang et al. 2017). Our photometric results of V342 UMa, such as the less massive component being the hotter one, and the reciprocal of our mass ratio is $1/q \sim 0.364$, are similar with those determined by Nelson et al. (2004). By collecting all of the available eclipsing times for V342 UMa and V509 Cam, we examined the period changes and found that the period of V342 UMa manifests a secular decrease at a rate of $-1.02(\pm0.54) \times 10^{-7}\,\mathrm{d\,yr^{-1}}$ and the period of V509 Cam is continuously increasing at a rate of $3.96(\pm0.90) \times 10^{-8}\,\mathrm{d\,yr^{-1}}$.

5.1 Absolute Parameter Estimation

Because of the lack of radial velocity curves for V342 UMa and V509 Cam, we cannot directly determine their absolute parameters. However, due to the *Gaia* mission (Gaia Collaboration et al. 2018), we can estimate the absolute parameters based on distance. First, the absolute magnitude of the two systems can be derived according to the parallax determined by the *Gaia* mission and the relation $M_V = m_V - 5\log D + 5 - A_V$, where m_V is the V band visual magnitude which can be referenced from Gettel et al. (2006), D represents the distance which can be computed by the *Gaia* parallax and A_V is extinction value which can be derived from Chen et al. (2018). Second, using equations $M_{\rm bol} = -2.5\log L/L_\odot + 4.74$ and $M_{\rm bol} = M_V + BC_V$ ($M_{\rm bol}$ is the absolute bolometric magnitude and BC_V is the bolometric correction which can be interpolated from table 5 in Pecaut & Mamajek (2013), the total luminosity of the binary can be calculated. Third, the luminosity of each component (L_1 and L_2) can be determined by the luminosity ratio L_2/L_1 listed in Table 3. Fourth, assuming blackbody emission ($L = 4\pi\sigma T^4 R^2$), the radius of each component can be estimated, hence the semimajor axis a can be obtained based the absolute and relative radius of each component (an average value of a was adopted). Finally, the mass of each component can be calculated by using Kepler's third law $M_1 + M_2 = 0.0134a^3/P^2$ and the mass ratio q. Following these steps, we computed the absolute param-

Table 2 Eclipsing Times of V342 UMa and V509 Cam

V342 UMa						V509 Cam					
HJD 2400000+	Errors	E	$O-C$	Residuals	References	HJD 2400000+	Errors	E	$O-C$	Residuals	References
53053.8040	0.0100	–3	–0.0014	–0.0010	[1]	51492.2770	–	0	–0.0013	0.0000	[15]
53053.9740	0.0100	–2.5	–0.0033	–0.0029	[1]	55937.8301	0.0003	12689	–0.0034	0.0001	[6]
53054.8371	0.0001	0	0.0001	0.0006	[1]	55996.3387	0.0005	12856	–0.0028	0.0007	[7]
53055.3529	0.0003	1.5	0.0002	0.0006	[1]	55996.5138	0.0013	12856.5	–0.0029	0.0006	[7]
53055.5253	0.0002	2	0.0006	0.0011	[1]	56017.7080	0.0004	12917	–0.0047	–0.0012	[6]
53057.7602	0.0002	8.5	0.0005	0.0009	[1]	57692.3700	0.0002	17697	–0.0021	0.0005	[16]
53057.9317	0.0002	9	0.0001	0.0005	[1]	57692.5435	0.0003	17697.5	–0.0038	–0.0012	[16]
53058.9635	0.0002	12	0.0003	0.0007	[1]	58158.3319	0.0002	19027	–0.0020	0.0003	[14]
53059.6509	0.0010	14	0.0000	0.0004	[1]	58158.5069	0.0001	19027.5	–0.0022	0.0001	[14]
53066.8716	0.0006	35	–0.0002	0.0002	[1]	58183.3815	0.0002	19098.5	–0.0022	0.0000	[14]
53067.0450	0.0006	35.5	0.0013	0.0017	[1]	58184.0819	0.0002	19100.5	–0.0025	–0.0002	[14]
53074.7807	0.0003	58	0.0003	0.0007	[1]	58184.2575	0.0002	19101	–0.0021	0.0002	[14]
53074.9528	0.0003	58.5	0.0005	0.0009	[1]	58184.4323	0.0002	19101.5	–0.0024	–0.0002	[14]
53077.7032	0.0003	66.5	0.0001	0.0005	[1]	58224.1969	0.0001	19215	–0.0022	0.0000	[14]
53077.8758	0.0002	67	0.0007	0.0011	[1]	58224.3725	0.0002	19215.5	–0.0018	0.0004	[14]
53404.8790	0.0002	1018	0.0009	0.0006	[2]	58232.2550	0.0002	19238	–0.0022	0.0001	[14]
53837.4389	0.0015	2276	–0.0049	–0.0015	[3]	58505.3504	0.0001	20017.5	–0.0023	–0.0004	[14]
54435.9180	0.0001	4016.5	0.0001	–0.0025	[4]						
54438.6690	0.0009	4024.5	0.0003	0.0015	[3]						
54499.8744	0.0002	4202.5	0.0001	0.0017	[5]						
54815.8735	0.0002	5121.5	–0.0007	0.0005	[5]						
55958.8411	0.0005	8445.5	0.0034	–0.0007	[6]						
56009.3875	0.0046	8592.5	0.0036	0.0046	[7]						
56009.5583	0.0039	8593	0.0025	0.0005	[7]						
56013.6833	0.0002	8605	0.0012	–0.0010	[6]						
56042.7440	0.0006	8689.5	0.0065	–0.0010	[6]						
56387.4512	0.0045	9692	0.0022	–0.0018	[8]						
56390.3725	0.0016	9700.5	0.0008	–0.0011	[8]						
56761.3883	0.0011	10779.5	0.0004	0.0201	[9]						
56783.3940	0.0012	10843.5	–0.0004	–0.0014	[9]						
57091.4856	0.0019	11739.5	0.0000	–0.0004	[10]						
57390.2931	–	12608.5	0.0002	–0.0012	[11]						
57450.2943	–	12783	–0.0007	0.0025	[11]						
57797.0720	–	13791.5	0.0024	–0.0076	[12]						
57797.2339	–	13792	–0.0076	–0.0014	[12]						
57806.8894	0.0003	13820	0.0200	–0.0024	[13]						
57817.1834	–	13850	–0.0016	–0.0019	[12]						
58207.1096	0.0003	14984	–0.0033	–0.0002	[14]						
58247.3406	0.0003	15101	–0.0030	–0.0015	[14]						
58260.2368	0.0004	15138.5	–0.0013	–0.0017	[14]						
58481.3317	0.0001	15781.5	–0.0030	–0.0016	[14]						
58504.1976	0.0002	15848	–0.0033	–0.0058	[14]						
58504.3696	0.0002	15848.5	–0.0032	–0.0012	[14]						

[1] Nelson et al. (2004); [2] Krajci (2006); [3] This paper (WASP); [4] Nelson (2008); [5] Nelson (2009); [6] Diethelm (2012); [7] Hubscher et al. (2013); [8] Hubscher (2014); [9] Hubscher & Lehmann (2015); [10] Hubscher (2016); [11] VSOLJ 63; [12] VSOLJ 64; [13] Nelson (2018); [14] This paper (WHOT); [15] Khruslov (2006); [16] OEJV 0179.

eters of V342 UMa and V509 Cam. The absolute parameters, along with the parameters needed in the calculation process, are provided in Table 4. This method provides an opportunity to estimate absolute parameters of contact binaries without radial velocity curve observations and can be applied to other contact binaries with reliable photometric solutions.

5.2 The Secular Period Changes

The period of V342 UMa exhibits a secular decrease at a rate of $-1.02(\pm0.54) \times 10^{-7}\,\mathrm{d\,yr^{-1}}$. Usually, the long-term period decrease is produced by conservative mass transfer or AML. If it is caused by conservative mass transfer, the mass transfer rate can be determined to be $dM_1/dt = 3.01(\pm1.59)\times10^{-8}\,M_\odot\ \mathrm{yr}^{-1}$ by using the following equation,

$$\frac{\dot{P}}{P} = -3\dot{M}_1(\frac{1}{M_1} - \frac{1}{M_2}). \quad (6)$$

The positive sign indicates that the less massive primary component is receiving mass. Assuming the angular momentum and total mass are constant and the more massive component transfers its mass on a thermal timescale, $\tau_{\rm th} = 3.39 \times 10^7$ yr can be calculated using the relation $\tau_{\rm th} = \frac{GM_2^2}{R_2 L_2}$. Then, the mass transfer rate can be roughly derived

Table 3 Photometric Results of V342 UMa and V509 Cam

Star	V342 UMa		V509 Cam		
Parameters	201901	201805	201803	201802	201804
T_1(K)	5902 ± 6	5899 ± 8	6523 ± 4	6498 ± 5	6560 ± 5
T_2(K)	5662 ± 11	5663 ± 16	6433 ± 9	6446 ± 12	6415 ± 11
q	2.748 ± 0.015	2.748(fixed)	2.549 ± 0.016	2.549(fixed)	2.549(fixed)
$i(^\circ)$	84.2 ± 0.2	82.9 ± 0.3	82.1 ± 0.1	82.3 ± 0.1	82.8 ± 0.2
L_2/L_1	2.040 ± 0.113	2.024 ± 0.110	2.145 ± 0.037	2.202 ± 0.023	2.073 ± 0.058
$\Omega_1 = \Omega_2$	6.219 ± 0.019	6.164 ± 0.006	5.816 ± 0.021	5.821 ± 0.005	5.828 ± 0.005
r_1	0.299 ± 0.001	0.305 ± 0.001	0.321 ± 0.001	0.319 ± 0.001	0.320 ± 0.001
r_2	0.476 ± 0.002	0.480 ± 0.001	0.481 ± 0.003	0.481 ± 0.001	0.481 ± 0.001
f	$10.0 \pm 3.1\%$	$19.0 \pm 1.0\%$	$32.1 \pm 3.4\%$	$31.3 \pm 0.9\%$	$30.1 \pm 0.9\%$
Spot	On Star 1	On Star 1	–	On Star 2	On Star 1
θ(radian)	1.273 ± 0.092	1.759 ± 0.212	–	0.467 ± 0.107	0.583 ± 0.132
ϕ(radian)	5.896 ± 0.064	2.134 ± 0.056	–	1.225 ± 0.057	1.658 ± 0.039
r(radian)	0.258 ± 0.069	0.358 ± 0.085	–	0.298 ± 0.064	0.423 ± 0.086
$T_f(T_d/T_0)$	0.832 ± 0.099	0.789 ± 0.124	–	0.811 ± 0.089	0.824 ± 0.078

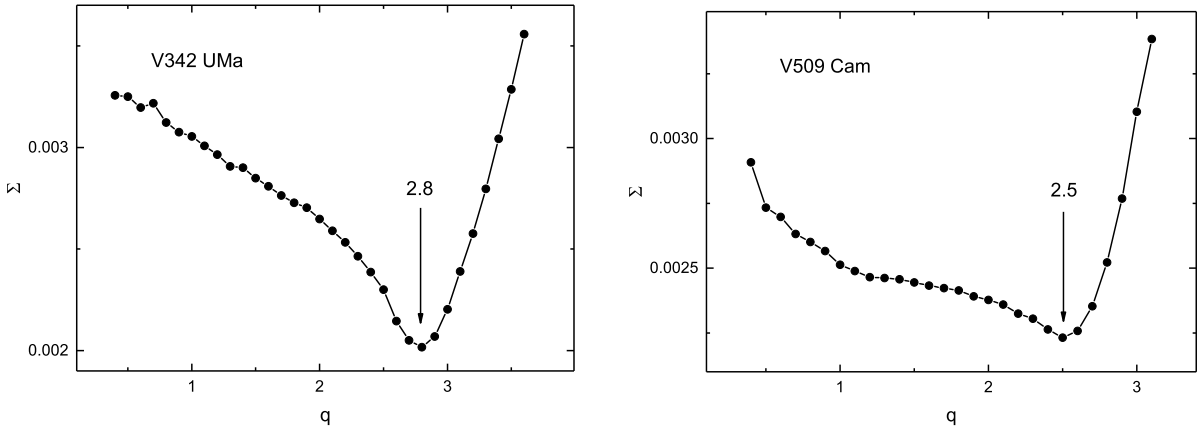

Fig. 4 This figure displays the $\sum W_i(O-C)_i^2$ versus mass ratio q of V342 UMa and V509 Cam.

Table 4 Absolute Parameters of V342 UMa and V509 Cam

Parameters	D (pc)	$V_{\max}$ (mag)	M_V (mag)	BC_V (mag)	$M_{\rm bol}$ (mag)	L_1 ($L_\odot$)	L_2 ($L_\odot$)	R_1 ($R_\odot$)	R_2 ($R_\odot$)	a ($R_\odot$)	M_1 ($M_\odot$)	M_2 ($M_\odot$)
V342 UMa	685.6	13.418	4.134	−0.115	4.019	0.640	1.303	0.766	1.188	2.530	0.490	1.293
	±14.0	–	±0.044	–	±0.044	±0.090	±0.157	±0.054	±0.072	±0.175	±0.103	±0.291
V509 Cam	674.0	12.933	3.647	−0.041	3.606	0.904	1.938	0.746	1.122	2.328	0.388	0.997
	±8.6	–	±0.028	–	±0.028	±0.068	±0.134	±0.028	±0.039	±0.093	±0.048	±0.129

to be $M_2/\tau_{\rm th} = 3.81 \times 10^{-8}\,M_\odot\,{\rm yr}^{-1}$, which coincides with the result determined by Equation (6). Another possibility is AML due to magnetic stellar winds. An approximation for calculating the period decrease rate was given by Guinan & Bradstreet (1998) as follows,

$$\frac{dP}{dt} \approx -1.1 \times 10^{-8} q^{-1}(1+q)^2(M_1+M_2)^{-5/3}k^2 \times (M_1R_1^4 + M_2R_2^4)P^{-7/3}, \quad (7)$$

where k^2 is the gyration constant. Taking $k^2 = 0.1$ from Webbink (1976) for low-mass main sequence stars, we inferred that the period decrease rate caused by AML is $-0.71 \times 10^{-7}\,{\rm d\,yr}^{-1}$, which is similar to the observed value. Therefore, both conservative mass transfer and AML can explain the long-term period decrease of V342 UMa. At present, we cannot know which one is dominant only based on the observed period variation.

The period of V509 Cam is continuously increasing at a rate of $3.96(\pm0.90) \times 10^{-8}\,{\rm d\,yr}^{-1}$. The long-term period increase is generally attributed to conservative mass transfer. Using Equation (6), we concluded that the mass transfer rate is $dM_1/dt = -1.07(\pm0.24)\times10^{-8}\,M_\odot\,{\rm yr}^{-1}$. The negative sign signifies that the less massive primary component is transferring mass to the more massive secondary one. V509 Cam is a late type contact binary, and

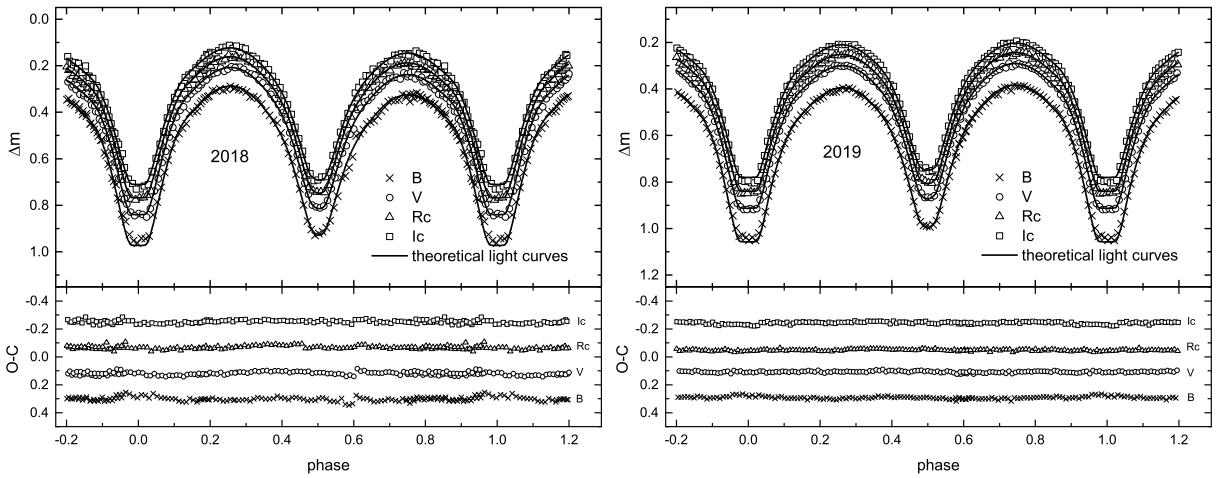

Fig. 5 A comparison between the synthetic and observed light curves for V342 UMa.

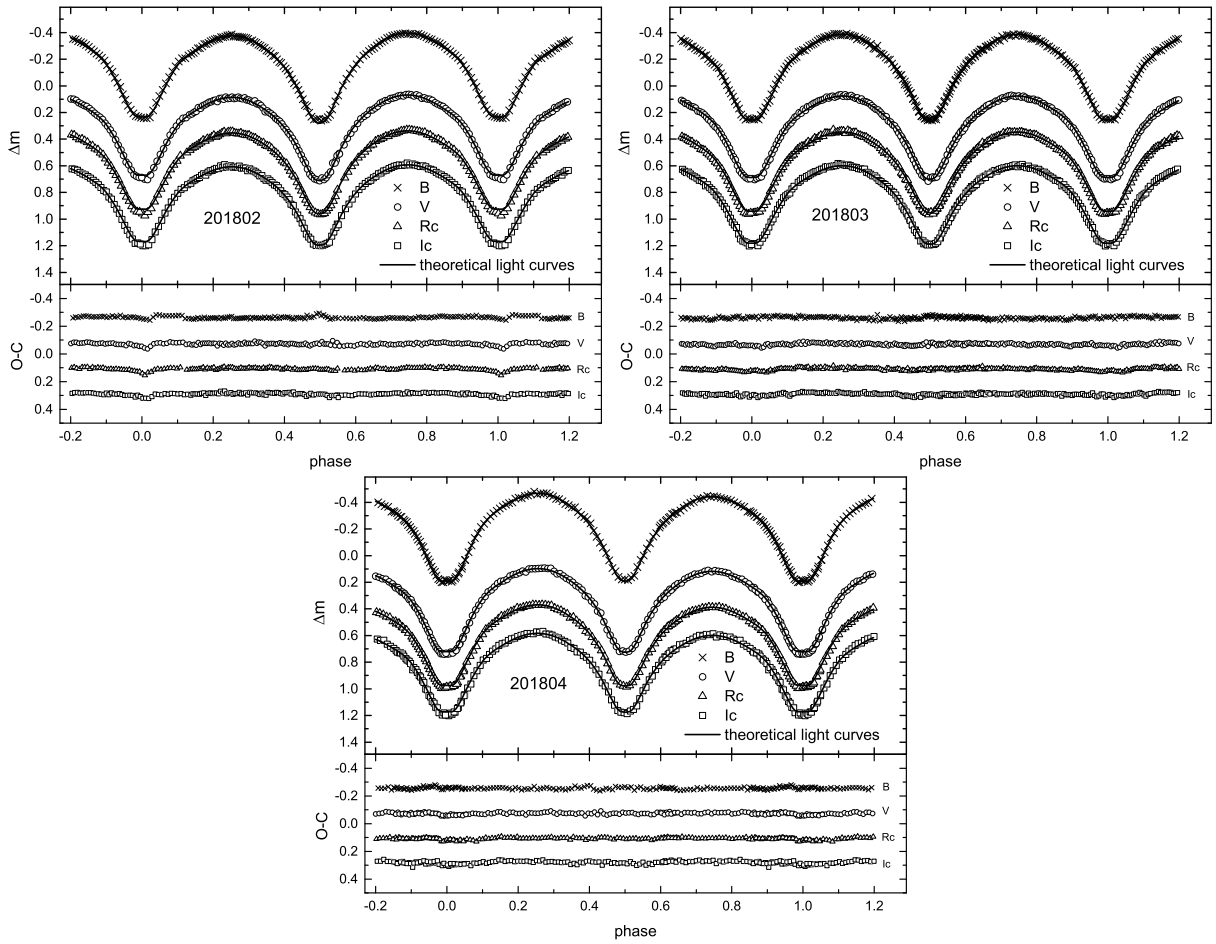

Fig. 6 A comparison between the synthetic and observed light curves for V509 Cam.

AML due to magnetic stellar winds can also happen in V509 Cam. Therefore, the determined mass transfer rate should be considered as a minimal value.

The secular period decrease rate, $-1.02(\pm0.54) \times 10^{-7}\,\mathrm{d\,yr^{-1}}$, of V342 UMa is very common in W-subtype contact binaries, such as $-1.69 \times 10^{-7}\,\mathrm{d\,yr^{-1}}$ for V502 Oph (Zhou et al. 2016), $-0.62 \times 10^{-7}\ \mathrm{d\,yr^{-1}}$

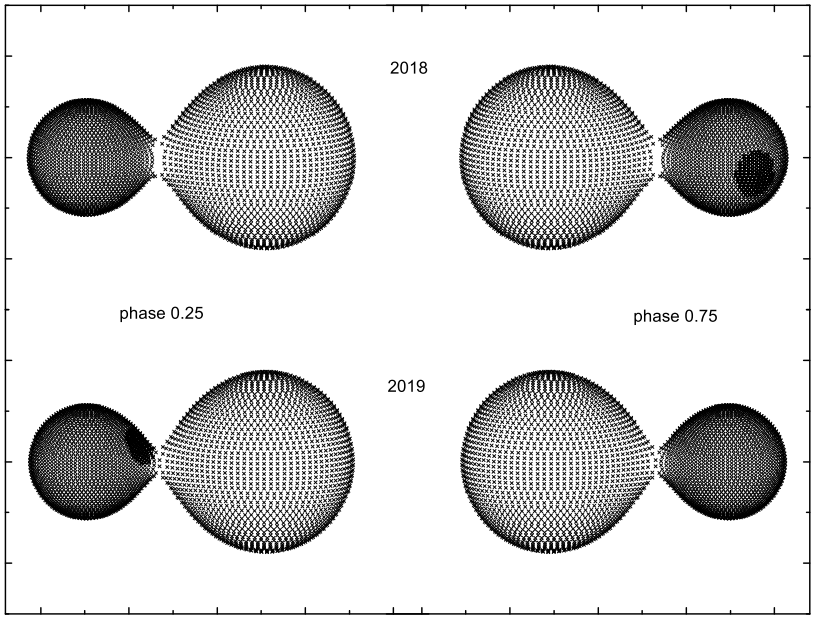

Fig. 7 Geometrical configurations of V342 UMa.

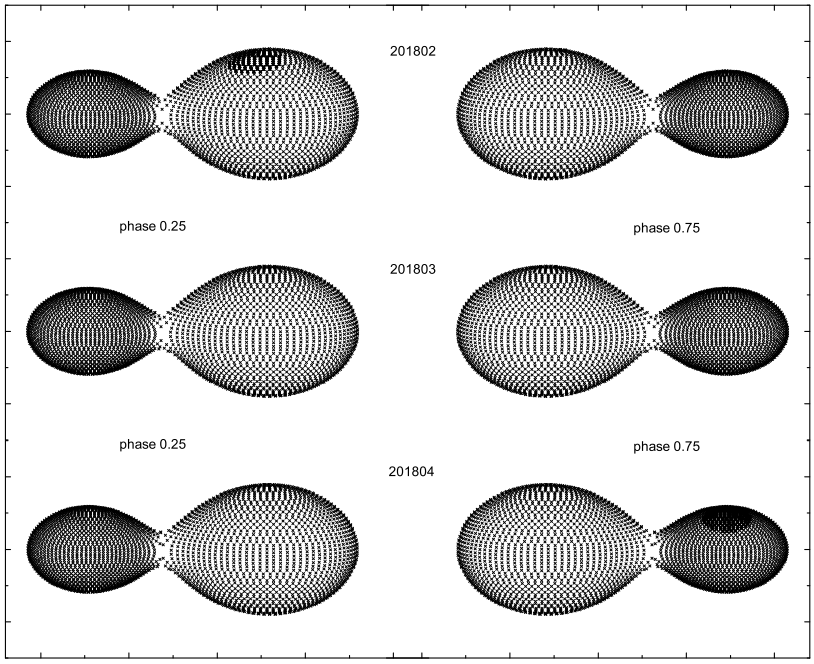

Fig. 8 Geometrical configurations of V509 Cam.

for GU Ori (Zhou et al. 2018) and $-1.78 \times 10^{-7}\,\mathrm{d\,yr^{-1}}$ for V1007 Cas (Li et al. 2018). With decreasing period, V342 UMa will evolve from the present shallow contact configuration to high fill-out contact state. The long-term period increase rate, $3.96(\pm0.90) \times 10^{-8}\,\mathrm{d\,yr^{-1}}$, of V509 Cam is also very common in W-subtype contact binaries, such as $5.09 \times 10^{-8}\,\mathrm{d\,yr^{-1}}$ for EP And (Lee et al. 2013), $7.7 \times 10^{-8}\,\mathrm{d\,yr^{-1}}$ for UX Eri (Qian et al. 2007b) and $6.5 \times 10^{-8}\,\mathrm{d\,yr^{-1}}$ for LR Cam (Yang & Dai 2010). With increasing period, V509 Cam may evolve into a broken-contact binary. There is another possibility that the long-term period variations of the two systems are only part of very long period periodic variations that result from a distant third body (Liao & Qian 2010), and continuous observations of the two targets are required to confirm this in the future.

Table 5 Light Differences for V342 UMa and V509 Cam at Different Epochs

Epoch	Filter	Min. I – Min. II	Max. II – Max. I	Min. I – Max. I	Min. II – Max. I
V342 UMa					
2018 May	B	0.041	0.034	0.673	0.632
	V	0.027	0.031	0.631	0.604
	R_c	0.020	0.027	0.607	0.587
	I_c	0.038	0.026	0.609	0.571
2019 Jan	B	0.055	–0.012	0.655	0.600
	V	0.043	–0.009	0.614	0.572
	R_c	0.036	–0.008	0.591	0.555
	I_c	0.045	–0.007	0.584	0.539
V509 Cam					
2018 Feb	B	–0.008	–0.021	0.620	0.628
	V	–0.007	–0.018	0.611	0.618
	R_c	0.000	–0.016	0.605	0.605
	I_c	0.004	–0.015	0.593	0.588
2018 Mar	B	–0.004	0.001	0.642	0.646
	V	–0.009	–0.001	0.610	0.619
	R_c	0.003	0.000	0.608	0.605
	I_c	0.003	0.000	0.591	0.588
2018 Apr	B	0.007	0.026	0.660	0.653
	V	0.013	0.021	0.641	0.628
	R_c	0.012	0.018	0.621	0.609
	I_c	0.021	0.016	0.613	0.592

Min. I, Min. II, Max. I, and Max. II respectively denote the primary light minimum, the secondary light minimum, the light maximum after Min. I and the light maximum after Min. II.

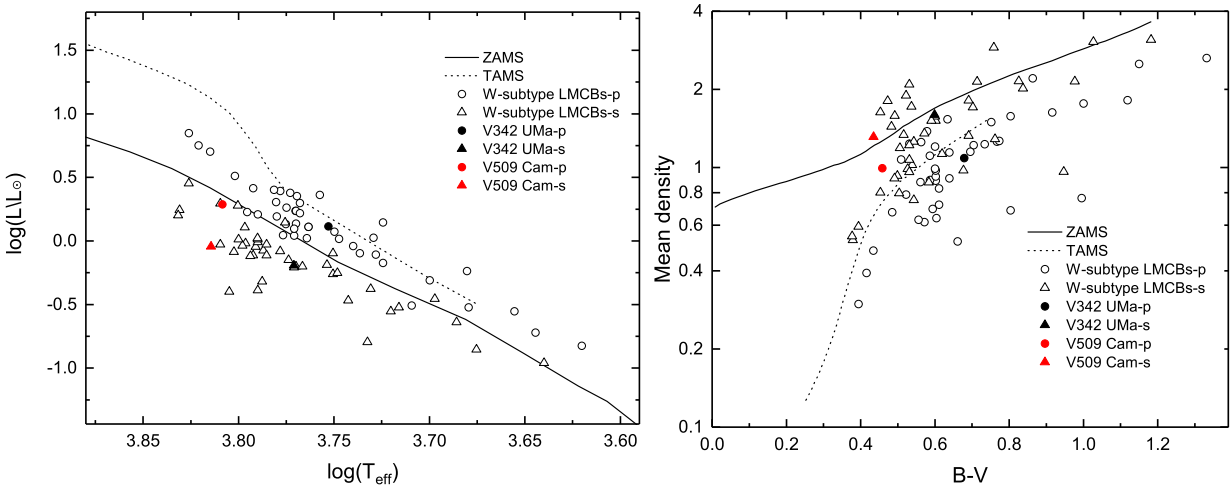

Fig. 9 The H-R diagram (*left*) and C-D diagram (*right*). The *solid* and *dotted lines* display the ZAMS and TAMS, respectively. The *circles* refer to the more massive components (p), while the *triangles* represent the less massive ones (s).

5.3 Light Curve Variations of the Two Targets

As seen in Figures 1 and 2, we can ascertain that the light curves of V342 UMa and V509 Cam display very clear variations. For V342 UMa, the light curves observed in 2018 show a positive O'Connell effect (which means the first light maximum, Max. I, is brighter than the second one, Max. II), while the light curves observed in 2019 reversed to exhibit a negative O'Connell effect (which means Max. I is fainter than Max. II). For V509 Cam, the light curves observed in February, 2018 manifest a negative O'Connell effect, then the light curves observed in March, 2018 are almost symmetric. However, the light curves reversed to exhibit a positive O'Connell effect in April, 2018. The differences between Min. I and Min. II, Max. II and Max. I, Min. I and Max. I, and Min. II and Max. I were calculated and are listed in Table 5. Such changes in the light curves are very common in contact binaries, such as BX Peg (Lee et al. 2004, 2009), HH UMa (Wang et al. 2015) and RT LMi (Qian et al. 2008). They are generally caused by magnetic activities and can be interpreted by the presence of spots. The changes in the light curves of V342 UMa and V509 Cam can both be explained by spot variation.

5.4 The Evolutionary Status

To study the evolutionary status of the two stars, the Hertzsprung-Russell (H-R) diagram and the color-density (C-D) diagram were constructed and are shown in the left and right panels of Figure 9, respectively. The zero age main sequence (ZAMS) and terminal age main sequence (TAMS) in the H-R diagram were taken from Girardi et al. (2000), while the ZAMS and TAMS in the C-D diagram come from Mochnacki (1981). In order to compare with other W-subtype contact binaries, the W-subtype low mass contact binaries (LMCBs) listed in Yakut & Eggleton (2005) are also displayed in Figure 9. The horizontal axis of the right panel in Figure 9 is color index, and we converted the temperatures of the components of all systems including V342 UMa and V509 Cam to color index based on table 5 of Pecaut & Mamajek (2013). The mean densities of the components were calculated using the relation provided by Mochnacki (1981),

$$\begin{aligned} \overline{\rho_1} &= \frac{0.079}{V_1(1+q)P^2}\,\mathrm{g\,cm^{-3}}, \\ \overline{\rho_2} &= \frac{0.079q}{V_2(1+q)P^2}\,\mathrm{g\,cm^{-3}}. \end{aligned} \tag{8}$$

In Figure 9, the ZAMS and TAMS are labeled as solid and dotted lines, respectively, and the circles refer to the more massive components (p), while the triangles represent the less massive ones (s). Both the H-R diagram and C-D diagram demonstrate that the components of V342 UMa and V509 Cam are consistent with those of other W-subtype contact systems. The less massive components are close to the ZAMS, meaning that they are main-sequence or little evolved stars, while the more massive ones are located near the TAMS, indicating that they are at an advanced evolutionary stage. The evolutionary status of the components of W-subtype contact systems is similar with that of the A-subtype ones. Therefore, the W-subtype phenomenon is still an open question. More observations and investigations of these two subtype contact binaries are needed.

In this paper, investigations of the light curves and period variations of V342 UMa and V509 Cam are presented. We found that both of the two systems are W-subtype contact binaries and manifest very strong light curve changes. The period change analysis reveals that V342 UMa displays long-term period decrease which can be caused by conservative mass transfer or AML due to magnetic stellar winds and that V509 Cam exhibits long-term period increase which can be attributed to conservative mass transfer. The absolute parameters of the two binaries were obtained based on the *Gaia* distances. To identify their cyclic period changes, further observations are required.

Acknowledgements This work is supported by the National Natural Science Foundation of China (No. 11703016), the Joint Research Fund in Astronomy (No. U1431105) under cooperative agreement between the National Natural Science Foundation of China and the Chinese Academy of Sciences, the program of the Light in China's Western Region (No. 2015-XBQN-A-02), the Natural Science Foundation of Shandong Province (Nos. ZR2014AQ019 and JQ201702), the Young Scholars Program of Shandong University, Weihai (Nos. 20820162003 and 20820171006), the program of Tianshan Youth (No. 2017Q091), and the Open Research Program of Key Laboratory for the Structure and Evolution of Celestial Objects (No. OP201704). Great thanks go the referee for very helpful comments and suggestions that improved our manuscript.

We acknowledge the support of the staff of the Xinglong 85-cm telescope, NOWT, WHOT and NEXT. This work was partially supported by the Open Project Program of the Key Laboratory of Optical Astronomy, National Astronomical Observatories, Chinese Academy of Sciences.

This paper makes use of data from the DR1 of the WASP data (Butters et al. 2010) as provided by the WASP consortium, and the computing and storage facilities at the CERIT Scientific Cloud, reg. no. CZ.1.05/3.2.00/08.0144 which is operated by Masaryk University, Czech Republic.

This work has made use of data from the European Space Agency (ESA) mission *Gaia* (`https://www.cosmos.esa.int/gaia`), processed by the *Gaia* Data Processing and Analysis Consortium (DPAC, `https://www.cosmos.esa.int/web/gaia/dpac/consortium`). Funding for the DPAC has been provided by national institutions, in particular the institutions participating in the *Gaia* Multilateral Agreement.

References

Bradstreet, D. H., & Guinan, E. F. 1994, in ASP Conf. Ser. 56, Interacting Binary Stars, ed. Allen W. Shafter (San Francisco, CA: ASP), 228

Butters, O. W., West, R. G., Anderson, D. R., et al. 2010, A&A, 520, 10

Chen, X., Deng, L., de Grijs, R., Wang, S., & Feng, Y. 2018, ApJ, 859, 140

Coughlin, J. L., Lopez, M. M., Harrison, T. E., Ule, N., & Hoffman, D. I. 2011, AJ, 141, 78

Dall, T. H., & Schmidtobreick, L. 2005, A&A, 429, 625

Diethelm, R. 2012, IBVS, 6029, 1

Dimitrov, D. P., & Kjurkchieva, D. P. 2015, MNRAS, 448, 2890

Eggleton, P. P., & Kisseleva-Eggleton, L. 2006, Ap&SS, 304, 75

Fabrycky, D., & Tremaine, S. 2007, ApJ, 669, 1298

Gaia Collaboration, Prusti, T., de Bruijne, J. H. J., et al. 2016, A&A, 595, 1
Gaia Collaboration, Brown, A. G. A., Vallenari, A., et al. 2018, A&A, 616, 1
Gettel, S. J., Geske, M. T., & McKay, T. A. 2006, AJ, 131, 621
Girardi, L., Bressan, A., Bertelli, G., et al. 2000, A&AS, 141, 371
Guinan, E. F., & Bradstreet, D. H. 1988, in Formation and Evolution of Low Mass Stars, eds. A. K. Dupree, & M. T. V. T. Lago (Dordrecht: Kluwer), 345
Hu, S. M., Han, S. H., Guo, D. F., & Du, J. J. 2014, RAA (Research in Astronomy and Astrophysics), 14, 719
Hubscher, J. 2014, IBVS, 6118, 1
Hubscher, J. 2016, IBVS, 6157, 1
Hubscher, J., Braune, W., & Lehmann, P. B. 2013, IBVS, 6048, 1
Hubscher, J., & Lehmann, P. B. 2015, IBVS, 6149, 1
Khruslov, A. V. 2006, PZP, 6, 11
Kjurkchieva, D. P., Popov, V. A., Eneva, Y., & Petrov, N. I. 2019a, RAA (Research in Astronomy and Astrophysics), 19, 14
Kjurkchieva, D., Stateva, I., Popov, V. A., & Marchev, D. 2019b, AJ, 157, 73
Krajci, T. 2006, IBVS, 5690, 1
Kwee, K. K. & van Woerden, H. 1956, BAN, 12, 327
Lee, J. W., Hinse, T. C., & Park, J.-H. 2013, AJ, 145, 100
Lee, J. W., Kim, C.-H., Han, W., Kim, H.-I., & Koch, R. H. 2004, MNRAS, 352, 1041
Lee, J. W., Kim, S.-L., Lee, C.-U., & Youn, J.-H. 2009, PASP, 121, 1366
Li, K., Xia, Q.-Q., Hu, S.-M., et al. 2018, PASP, 130, 074201
Liao, W.-P., & Qian, S.-B. 2010, MNRAS, 405, 1930
Liu, J., Zhang, Y., Feng, G., & Bai, C. 2014 in IAU Symp., 298, Setting the Scene for Gaia and LAMOST, eds. S. Feltzing et al. (Cambridge: Cambridge Univ. Press), 427
Lucy, L. B. 1967, Z. Astrophys. 65, 89
Mochnacki, S. W. 1981, ApJ 245, 650
Nelson, R. H. 2008, IBVS, 5820, 1
Nelson, R. H. 2009, IBVS, 5875, 1
Nelson, R. H. 2018, IBVS, 6234, 1
Nelson, R. H., Henden, A. A., & Krajci, T. 2004, IBVS, 5546, 1
Pecaut, M. J., & Mamajek, E. E. 2013, ApJS, 208, 9
Pribulla, T., Kreiner, J. M., & Tremko, J. 2003, CoSka, 33, 38
Qian, S.-B., He, J.-J., Xiang, F.-Y. 2008, PASJ, 60, 77
Qian, S.-B., He, J.-J., Zhang, J. et al. 2017, RAA (Research in Astronomy and Astrophysics), 17, 87
Qian, S.-B., Wang, J.-J., Zhu, L.-Y., Snoonthornthum, B., Wang, L.-Z., Zhao, E. G., Zhou, X., Liao, W.-P., & Liu, N.-P. 2014, ApJS, 212, 4
Qian, S.-B., Yang, Y.-G., Zhu, L.-Y., He, J.-J., & Yuan, J.-Z. 2006, Ap&SS, 304, 25
Qian, S.-B., Yuan, J.-Z., Soonthornthum, B., et al. 2007a, ApJ, 671, 811
Qian, S.-B., Yuan, J.-Z., Xiang, F.-Y. et al. 2007b, AJ, 134, 1769
Qian, S.-B., Zhang, J., He, J.-J. et al. 2018, ApJS, 235, 5
Ruciński, S. M. 1969, Acta Astronomica, 19, 245
Rucinski, S. M. 2010, AIPC, 1314, 29
Terrell, D., & Wilson, R. E. 2005, Ap&SS 296, 221
van Hamme, W. 1993, AJ, 106, 2096
Wang, K., Zhang, X. B., Deng, L. C., et al. 2015, ApJ, 805, 22
Webbink, R. E. 1976, ApJ, 209, 829
Wilson, R. E. 1979, ApJ, 234, 1054
Wilson, R. E. 1990, ApJ, 356, 613
Wilson, R. E., & Devinney, E. J. 1971, ApJ, 166, 605
Yakut, K., & Eggleton, P. P. 2005, ApJ, 629, 1055
Yang, Y.-G., & Dai, H.-F. 2010, PASJ, 62, 1045
Zhang, J., Qian, S. B., Han, Z. T., Wu, Y. 2017, MNRAS, 466, 1118
Zhou, X., Qian, S. B., Boonrucksar, S., et al. 2018, PASJ, 70, 87
Zhou, X., Qian, S. B., Huang, B., et al. 2016, PASJ, 68, 102